



## **Straightforward prediction of the Ni<sub>1-x</sub>O layers stoichiometry by using optical and electrochemical measurements**

Laura Maria Manceri, Pierre Colson, Anthony Maho, Gauthier Eppe, Ngoc Duy Nguyen, Christine Labrugère, Aline Rougier, Rudi Cloots, Catherine Henrist

### **► To cite this version:**

Laura Maria Manceri, Pierre Colson, Anthony Maho, Gauthier Eppe, Ngoc Duy Nguyen, et al.. Straightforward prediction of the Ni<sub>1-x</sub>O layers stoichiometry by using optical and electrochemical measurements. *Journal of Physics D: Applied Physics*, 2017, 50 (22), 225501 (12 p.). 10.1088/1361-6463/aa6e71 . hal-01545821

**HAL Id: hal-01545821**

**<https://hal.science/hal-01545821>**

Submitted on 9 Feb 2021

**HAL** is a multi-disciplinary open access archive for the deposit and dissemination of scientific research documents, whether they are published or not. The documents may come from teaching and research institutions in France or abroad, or from public or private research centers.

L'archive ouverte pluridisciplinaire **HAL**, est destinée au dépôt et à la diffusion de documents scientifiques de niveau recherche, publiés ou non, émanant des établissements d'enseignement et de recherche français ou étrangers, des laboratoires publics ou privés.

# **Straightforward prediction of the $\text{Ni}_{1-x}\text{O}$ layers stoichiometry by using optical and electrochemical measurements**

Laura Maria MANCERIU<sup>a,\*</sup>, Pierre COLSON<sup>a</sup>, Anthony MAHO<sup>a,g</sup>, Gauthier EPPE<sup>b</sup>, Ngoc Duy NGUYEN<sup>c</sup>, Christine LABRUGERE<sup>d</sup>, Aline ROUGIER<sup>e</sup>, Rudi CLOOTS<sup>a</sup>, Catherine HENRIST<sup>a,f</sup>

<sup>a</sup>University of Liège, UR CESAM, GREENMat, Quartier AGORA, Allée du Six-Août 13, BE-4000 Liège (Sart-Tilman), Belgium.

<sup>b</sup>University of Liège, Chemistry Departement, Analytical Chemistry and Electrochemistry, Quartier AGORA, Allée du Six-Août 13, BE-4000 Liège (Sart-Tilman), Belgium

<sup>c</sup>University of Liege, Physics Department, CESAM/Q-MAT, SPIN, B-4000 Liege, Belgium

<sup>d</sup>CNRS, Université de Bordeaux, PLACAMAT UMS 3626, F-33600 Pessac, France

<sup>e</sup>CNRS, Université de Bordeaux, ICMCB, UPR 9048, F-33600Pessac, France

<sup>f</sup> Cellule d'Appui à la Recherche et à l'Enseignement en Microscopie ( CAREM) of the University of Liege, Quartier AGORA, Allée du Six-Août 13, BE-4000 Liège (Sart-Tilman), Belgium

<sup>g</sup>Fonds de la Recherche Scientifique – FNRS, Rue d'Egmont 5, BE-1000 Brussels, Belgium.

## **Abstract**

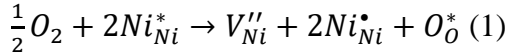
In this study, we propose a straightforward method for  $x$  determination in sub-stoichiometric nickel oxide ( $\text{Ni}_{1-x}\text{O}$ ) films prepared by ultrasonic spray pyrolysis on Fluor-Tin Oxide (FTO) substrates by varying the post-deposition thermal treatment. The  $\text{Ni}^{3+}$  concentration, the flat band potential ( $\Phi_{fb}$ ) and the open circuit potential ( $V_{oc}$ ) were determined by electrochemical impedance analysis in aqueous media and correlated to the transmission of as-deposited  $\text{Ni}_{1-x}\text{O}$  films. An X-Ray photoelectron spectroscopy study was also performed to quantify the amount of  $\text{Ni}^{3+}$  in the films and compare it with the one determined by electrochemical analysis. The electrochromic behavior of the  $\text{Ni}_{1-x}\text{O}$  films in non-aqueous electrolyte was investigated as well.

With increasing  $\text{Ni}^{3+}$  concentration the films became more brownish and more conductive, both  $V_{oc}$  and  $\Phi_{fb}$  values increased. Calibration curves of transmission at 550 nm or open circuit potential vs. carrier concentration were plotted and allowed the prediction of  $x$  in an unknown  $\text{Ni}_{1-x}\text{O}$  sample. The  $\text{Ni}_{1-x}\text{O}$  films characterized by the highest  $\text{Ni}^{3+}$  concentration have a darker colored state but lower transmission modulation, due to their reduced specific surface and increased crystallinity.

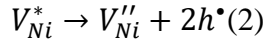
Key words: nickel oxide, thin films, stoichiometry evaluation, impedance spectroscopy, optical properties.

## 1. Introduction

Nickel oxide (NiO) is a wide band gap p-type semiconductor which is studied in a large range of applications, such as electrochromic coatings [1,2], new generation solar cells [3,4], gas sensors [5,6] or light-emitting diodes [7], due to its remarkable chemical stability, unique opto-electronic and magnetic properties. The p-type conductivity property is attributed to the presence of Ni vacancies and from here comes the notation  $Ni_{1-x}O$  (in addition described as  $NiO_y$  when oxygen interstitials are considered as the main defects [8]), where  $x < 10^{-3}$  [9,10], the defects being the expression of a departure from stoichiometry as function of oxygen partial pressure. According to P. Lunkenheimer et al. [11] the x maximum value is 0.2. In the form of thin films, the higher the x value is the more brownish the appearance will be. One nickel vacancy is compensated by the creation of two  $Ni^{3+}$  sites (eq. 1) and holes (eq. 2) [12], which provide both optical absorption and conductivity.



where,



where  $Ni_{Ni}^*$  stands for nickel atoms in their normal site,  $V_{Ni}''$  is the ionized nickel vacancy,  $V_{Ni}^*$  is the non-ionized nickel vacancy and  $Ni_{Ni}^{\bullet}$  is a  $Ni^{3+}$  site in a normal  $Ni^{2+}$  site,  $O_O^x$  represents the oxygen atoms in their normal site and  $h^{\bullet}$  are the holes.

Likewise, the excess oxygen in the nickel oxide lattice creates nickel vacancies which are ionized with the formation of  $Ni^{3+}$  sites and holes [13].

Nickel oxide is a well known anodic electrochromic material which reversibly switches from transparent to brownish by electrochemical reduction and oxidation, respectively. It was previously observed that the presence of Ni vacancies [2,14], influences the optical properties in the sense that a high initial  $Ni^{3+}$  content leads to lower transmission in the bleached and colored

states as well as to larger optical modulation [14,15]. In addition, Da Rocha and Rougier [15] observed that with increasing  $\text{Ni}^{3+}$  content the open circuit voltage increases along with film resistance decrease. This is not surprising since  $V_{oc}$  is a material property which represents in fact the chemical potential (Fermi level) of  $\text{Ni}_{1-x}\text{O}$  measured vs. the reference electrode.

Hence, it is important to find a method to determine the amount of  $\text{Ni}^{3+}$  in the  $\text{Ni}_{1-x}\text{O}$  films as they are involved in many different applications; first for electrochromic applications, where window transparency has to satisfy the customer needs and where the straightforward prediction of the coatings optical performance would be useful; then for p-type dye sensitized solar cells, where the conversion efficiency is directly dependent on the cell  $V_{oc}$  (potential difference between  $\text{Ni}_{1-x}\text{O}$  Fermi level and electrolyte Fermi level) and where tuning the material band structure is a key ingredient in increasing performance; or for gas sensors, where sensing performances of  $\text{Ni}_{1-x}\text{O}$  is strongly related to the intrinsic defect concentration.

Various chemical and physical approaches have been developed to produce  $\text{Ni}_{1-x}\text{O}$  films including spray pyrolysis [16,17], sputtering [15,18,19], pulsed laser deposition [20,21], atomic layer deposition [22], electrodeposition [23], chemical vapor deposition [24], etc. In parallel, different strategies were used to modify the  $\text{Ni}_{1-x}\text{O}$  stoichiometry such as annealing in oxygen rich or oxygen poor atmosphere [22,19,25], doping [16,22], modification of the  $\text{O}_2$  partial pressure [12,18], etc. Nevertheless, all these strategies lead to modifications in layer structure and morphology with important consequences on electrochemical measurements since the electrochemically active surface changes, which issue is rarely considered during elemental analysis. For investigating the  $\text{Ni}_{1-x}\text{O}$  stoichiometry, energy-dispersive X-ray spectroscopy (EDS), X-ray photoelectron spectroscopy (XPS), Rutherford Backscattering Spectrometry (RBS) or electrochemical methods are typically used.

EDX allows micrometer range profiling with medium detection sensitivity (0.1-1.0 at. %) but is mistakenly used to determine the O/Ni ratio since light elements like O cannot be properly quantified and is highly sensitive to surface roughness. XPS allows surface quantification (up to 10 nm), reaching even lower detection limits (0.1 at. %). However it is sensitive to organic contamination and quantitative determination of  $\text{Ni}^{3+}$  is still delicate because it is very much dependent on the fitting and calculation approach [12, 26]. RBS is considered more reliable than XPS due to the higher analysis depth (1  $\mu\text{m}$ ) with detection limits ranging from  $10^{-3}$  at. % for

heavy elements to 10 at. %. However, if not coupled with Nuclear Reaction Analysis (NRA), it can give false information about the oxygen content. Electrochemical methods like cyclic voltammetry or impedance spectroscopy rely on the proper selection of set-up and measuring conditions since these measurements are highly sensitive to sample or electrolyte contamination, defective contacts, analysis parameters (media, pH, scanning speed, etc.) or sample structure.

Given that the techniques have different capabilities, limitations, and depths of analysis, they can provide differing results even for highly homogenous films. Kim and Lee [18] have analyzed the stoichiometry of R.F. sputtered  $\text{Ni}_{1-x}\text{O}$  layers and observed that the content of  $\text{Ni}^{3+}$  is over estimated by XPS ( $x = 0.020$ ) with report to RBS ( $x = 0.006$ ). When analyzing the  $\text{Ni}_{1-x}\text{O}$  layers prepared by R.F. sputtering at  $P(\text{O}_2) = 6\%$ , Chen et. al [12] noted that the  $x$  values calculated from the O/Ni ratio are much lower ( $x = 0.076$ ) compared to  $x$  values derived from the  $\text{Ni}^{3+}/\text{Ni}^{2+}$  ratio ( $x = 0.13$ ). They explained this by  $\text{Ni}^{3+}$  enrichment at the surface of nanostructures. The  $x$  value determined from cyclic voltammetry curves [15] is much smaller ( $x = 0.035$ ) than the  $x$  value obtained by RBS [14] ( $x = 0.32$ , considering that for each oxygen interstitial one nickel vacancy is formed) for  $\text{Ni}_{1-x}\text{O}$  film with similar thickness, even if the pristine transmission level at 550 nm is lower (44% vs. 62%, respectively), suggesting higher  $\text{Ni}^{3+}$  content.

These facts are motivating our original approach, i.e. the prediction of the  $\text{Ni}_{1-x}\text{O}$  stoichiometry by using optical and electrochemical measurements. To be more specific, calibration curves of transmission or open circuit potential vs. carrier ( $\text{Ni}^{3+}$ ) concentration were constructed which allow predicting the amount of  $\text{Ni}^{3+}$  in an unknown sample just by measuring the initial transmission or the  $V_{oc}$ . The calibration relies on the linear dependence between transmission- $V_{oc}$ -carrier concentration, a dependence which was here established for the first time. This cheap, flexible and straightforward method can replace expensive and time consuming analysis such as XPS or RBS. A literature survey concerning  $\text{Ni}_{1-x}\text{O}$  stoichiometry determination is provided which allowed comparing our results with previous reports and evaluating the suitability of the different elemental analysis techniques.

## 2. Experimental part

### 2.1 Thin films preparation

Before deposition, the 2 cm x 2 cm FTO substrates (TEC15, 15 Ohm/sq., Dyesol) were degreased, rinsed with de-ionized water, followed by sonication treatments in ethanol and acetone baths for 6 min, and then blow-dried under compressed air stream. Ni<sub>1-x</sub>O thin films were deposited by ultrasonic spray pyrolysis (USP) at 350 °C from a 0.5M Ni(NO<sub>3</sub>)<sub>2</sub>•6H<sub>2</sub>O (Aldrich, 99.999%) solution to which polyethyleneglycol PEG (Aldrich, average M<sub>n</sub> 400) was added in mass ratio Ni(NO<sub>3</sub>)<sub>2</sub> : PEG = 1 : 3. As previously described [2], the USP equipment is an ExactaCoat<sup>®</sup> apparatus from Sonotek<sup>®</sup> equipped with an AccuMist<sup>®</sup> nozzle operated at 120 kHz, atomizing the solution into very fine droplets which are then conveyed by a carrier gas towards the heated substrate where the pyrolysis (precursor conversion and surfactant decomposition) takes place, forming the Ni<sub>1-x</sub>O films. The USP deposition parameters [2] involved a nozzle-substrate distance of 5.5 cm, a solution flow rate of 0.25 mL/min, and the use of air as carrier gas (6025 Pa). Deposition follows a “x,y” patterning above the surface with a S-shaped move (4 mm spacing) at a constant speed of 40 mm/s. The “x,y” deposition was performed 10 consecutive times, keeping exactly the same pattern every odd passages and shifting “x” (or “y”) coordinate by 2 mm every even passages. Likewise, deposition was done onto standard, non-conducting glass substrates for X-Ray characterization. After deposition, the Ni<sub>1-x</sub>O thin films were annealed at 350, 400, 500 and 600 °C in air for 3 h to modify their stoichiometry. Sample names correspond to the applied annealing temperatures.

## 2.2 Thin films characterization

The Ni<sub>1-x</sub>O coatings thickness was determined in cross-section by scanning electron microscopy (SEM) on an ESEM-FEG XL 30 FEI instrument, operated at 15 kV in the backscattered electron mode. The following values were obtained (average of 10 measurements): 293 ± 12 nm (350°C), 200 ± 13 nm (400°C), 242 ± 20 nm (500°C) and 202 ± 15 nm (600°C). Atomic Force Microscopy (AFM, Digital Instrument Nanoscope III microscope from Veeco) was also exploited to record surface topography of the Ni<sub>1-x</sub>O films and allowed for determining roughness and grain size distribution. The image acquisition was performed in tapping mode with a super sharp (tip diameter 5 nm) – improved super cone probe (Team Nanotec). Surface porosity was also evaluated through contact angle measurements (KSV instruments, static contact angle mode) using glycerol as testing liquid since water was readily absorbed by the porous samples and did not allow qualitative measurements. X-ray diffraction (XRD) was used to assess the crystalline nature of the Ni<sub>1-x</sub>O layers. Analysis were realized on a Bruker D8

Discovery diffractometer (grazing incidence, Cu K $\alpha$  radiation,  $\alpha = 0.154$  nm,  $32^\circ < 2\theta < 48^\circ$ , step width  $0.02^\circ$ , 1.5 s/step,  $2^\circ$  incidence angle).

A Thermo Fisher Scientific K-Alpha spectrometer (monochromatized AlK $\alpha$  source,  $h\nu=1486.6$  eV, spot size  $200\ \mu\text{m}$ ) was used for surface XPS analysis of the Ni $_{1-x}$ O thin films. The full spectra (0-1150 eV) were obtained with constant pass energy of 200 eV and high resolution spectra with constant pass energy of 40 eV. Quantification of Ni $^{3+}$  was done based on the fits of the high resolution Ni 2p $_{3/2}$  spectra using the AVANTAGE software (Thermo Fisher Scientific).

The Ni $_{1-x}$ O films resistance was studied by 2-points contact measurements (considering a vertical geometry, contact diameter 0.12 cm) using a PhysTech RH 2035 system. The carrier concentration, flat band potential and NiO/electrolyte interface properties were determined by electrochemical impedance spectroscopy analysis in aqueous media (0.1M NaH $_2$ PO $_4$  + 1M KCl, pH adjusted to 7 with NaOH to guarantee constant pH and ionic strength) in the 50 Hz - 800 kHz frequency range (51 points uniformly distributed over a logarithmic scale) under variable potential. In the case of Mott-Schottky measurements, the frequency scanning was started from the negative potential values towards positive values. Electrolyte solutions of pH 8, 9 and 10 were also prepared for studying the variation of the flat band potential with pH. The area of the electrode which was exposed to electrolyte was  $0.15\ \text{cm}^2$ . The electrolyte was purged with Ar for 30 min before the analysis to remove any dissolved oxygen. The electrochemical measurements were carried out in a custom three-electrode cell using a potentiostat (Biologic SP300 with frequency response analyzer), a platinum counter electrode, an Ag/AgCl in saturated KCl reference (0.248V vs. SHE, XR300 Radiometer Analytical) electrode for the aqueous media and an Ag/AgCl in 3M KCl saturated with AgCl (0.208V vs. SHE, REF361 Radiometer Analytical) for the non-aqueous media. The cyclic voltammetry and chronoamperometry experiments were carried out in a solution of lithium perchlorate 0.5 M (99.99%, Aldrich) in propylene carbonate (anhydrous 99.7%, Sigma Aldrich) in the -0.5 to 1.2V potential range. The absorption spectra of the initial, colored and bleached Ni $_{1-x}$ O films were registered using a Perkin Elmer Lambda 25 UV/VIS spectrometer in the 350 – 700 nm wavelength range (slit width 1 nm, beam cross section at focal point 0.6 mm x 9 mm) using air as blank. The contribution of the FTO substrate was subtracted from the initial absorption spectra of the annealed Ni $_{1-x}$ O films for more accurate correlation with the film composition.

### 3. Results and discussion

#### 3.1 Structural and morphological characterization

The X-Ray diffraction patterns of  $\text{Ni}_{1-x}\text{O}$  deposited onto standard glass annealed at different temperatures were acquired (Fig. 1) to evaluate temperature related changes in crystallinity and stoichiometry. The (1 1 1) and (2 0 0) X-ray peaks were observed at  $2\theta$  angles of approximately  $37.2^\circ$  and  $43.2^\circ$ , respectively, which constitutes a proof of cubic phase (PDF # 00 047 1049 from PDF-4+ database of International Center for Diffraction Data) formation. No evidence of  $\text{Ni}_2\text{O}_3$  or other phase formation was found. The average crystallite size for each sample was calculated for the (2 0 0) peak using the Debye-Scherrer formula:

$$D = \frac{0.9\lambda}{B\cos\theta} \quad (3)$$

where  $D$  is the crystallite size in nm,  $\lambda$  is the wavelength of the incident radiation ( $\text{Cu K}\alpha = 0.154$  nm),  $\theta$  is the Bragg angle and  $B$  is the FWHM of the diffraction peak in radians. The lattice constant “ $a$ ” was calculated with the following formula (standard deviation of calculated values is  $\pm 0.005$  nm):

$$a = d(h^2 + k^2 + l^2)^{1/2} \quad (4)$$

where  $h$ ,  $k$  and  $l$  are the Miller indices of the (2 0 0) peak and “ $d$ ” is the interplanar distance obtained from the Bragg law ( $d = \lambda/2\sin\theta$ ). Both “ $D$ ” and “ $a$ ” values are plotted in Fig. 1. The crystallinity of the  $\text{Ni}_{1-x}\text{O}$  films increases with increasing annealing temperature (Fig. 1a), with crystallites size ranging from around 9 nm to 21 nm. A slight shift of the patterns towards higher  $2\theta$  angles is observed ( $2\theta$  is  $43.19^\circ$ ,  $43.27^\circ$ ,  $43.32^\circ$  and  $43.33^\circ$  for sample 350, 400, 500 and 600, respectively), corroborated with the decreasing lattice parameter values (Fig. 1b).

Since the crystallite size increases, particle size increase is also expected and consequently changes in layer roughness. These aspects are very important for our approach since it was already shown that the  $\text{Ni}_{1-x}\text{O}$  electrochemically active surface is dependent on layer crystallinity and morphology [14]. The AFM images confirm the XRD results, i.e. the particle size increase with annealing temperature, with a granular morphology characterizing all the samples. Particle size distribution was calculated based on the AFM images by using the ImageJ software and



shown next to the topographies in Fig. 2. All layers were characterized by low roughness values (Fig. 2), slightly increasing when going from 400 to 600 °C annealing temperature due to particle size increase. The average particle sizes were slightly different than the crystallite sizes since the particles are polycrystalline and their size was calculated for the  $\text{Ni}_{1-x}\text{O}$  thin films deposited on different substrates, FTO and glass, respectively.

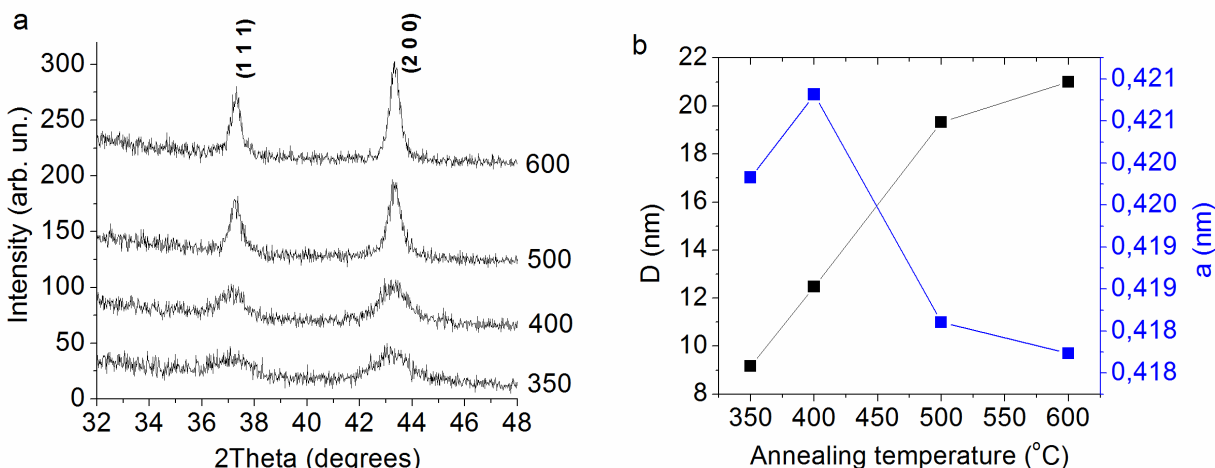


Fig. 1 X-Ray diffraction patterns (a) and crystallite size and lattice parameter (b) values of the  $\text{Ni}_{1-x}\text{O}$  films on glass substrate annealed at 350, 400, 500 and 600 °C for 3 h.

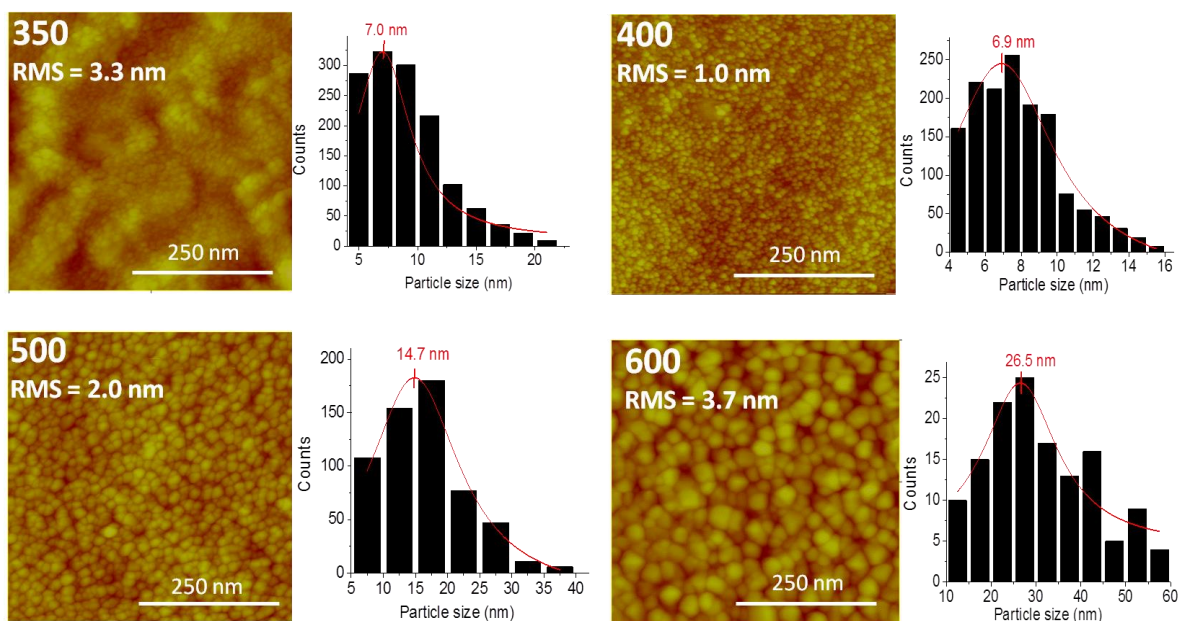


Fig. 2 AFM images (500 nm x 500 nm) and particle size distribution for the  $\text{Ni}_{1-x}\text{O}$  films annealed at 350, 400, 500 and 600 °C for 3 h. Roughness values are also shown on the pictures.

Contact angle measurements were performed on the  $\text{Ni}_{1-x}\text{O}$  film using glycerol as testing liquid since in the case of water the drop was readily absorbed. As it can be observed in Fig. 3 the glycerol contact angle is rather constant for the  $\text{Ni}_{1-x}\text{O}$  films annealed at 350 and 400 °C but increases for higher temperatures along with roughness increase. We suppose that is the combined effect of surface roughness, increasing film density and dehydroxylation of the surface. A rougher surface has an increased air trapping capability rendering a hydrophobic effect [27].

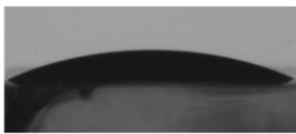
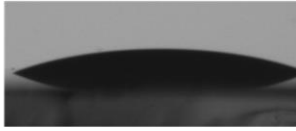
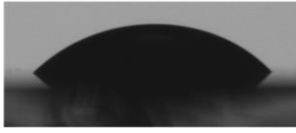

Sample	CA (°) glycerol	Image of the droplet on the surface
350	$24.0 \pm 5.2$	
400	$20.5 \pm 5.2$	
500	$44.2 \pm 2.2$	
600	$51.2 \pm 2.7$	

Fig. 3 Contact angle values of the  $\text{Ni}_{1-x}\text{O}$  films annealed at 350, 400, 500 and 600 °C for 3 h. Pictures of the glycerol droplet formed on the film surface are also shown for each case.

### 3.2 Optical properties

The absorption spectra of the  $\text{Ni}_{1-x}\text{O}$  films deposited on FTO were recorded versus air and normalized with the film thickness. The transmission spectra were obtained by mathematical conversion ( $T = 10^{2-A}$ ). The optical results confirm that the annealing was effective in modifying the  $\text{Ni}_{1-x}\text{O}$  film stoichiometry, i.e. absorption increases/transmission decreases (Fig. 4a and b) with increasing annealing temperature due to increasing  $\text{Ni}^{3+}$  concentration.

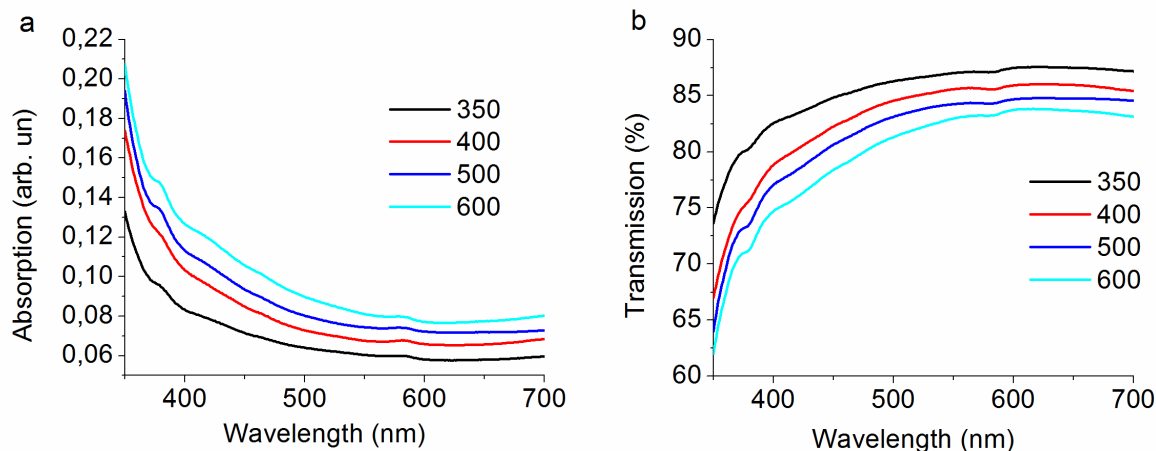


Fig. 4 Absorption (a) and transmission (b) spectra of the  $\text{Ni}_{1-x}\text{O}$  films annealed at 350, 400, 500 and 600°C for 3h.

### 3.3 Electrochemical and electrical properties

Given that in our approach we were searching a correlation between the optical and electrical/electrochemical properties, the carrier concentration ( $N$ ) was determined by Mott-Schottky analysis. Before that, electrochemical impedance spectroscopy was used to investigate the charge transfer properties at the  $\text{Ni}_{1-x}\text{O}$  film/ electrolyte interface. The Nyquist plots of  $\text{Ni}_{1-x}\text{O}$  samples are shown in Fig. 5a.

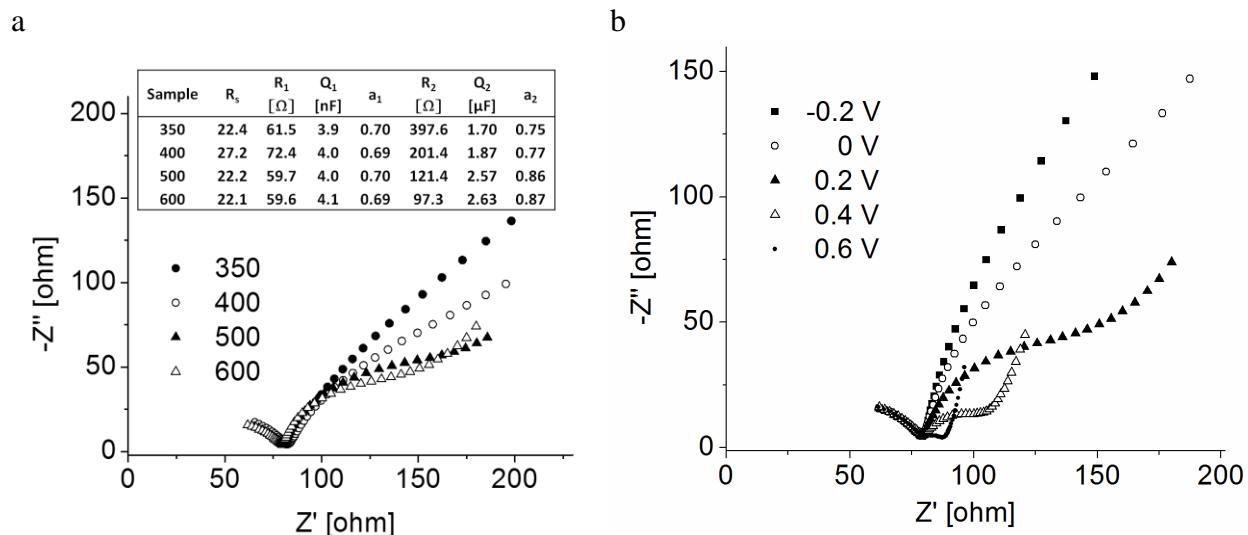


Fig. 5 Nyquist plots of the samples 350, 400, 500 and 600 at 0.2V (a), Nyquist plots of the sample 600 as function of applied potential (b).

At low annealing temperatures (samples 350 and 400 °C) a clear half-semicircle was visible in the high frequency range and the existence of a second depressed semicircle in the mid-frequency range could be distinguished. However, at higher annealing temperatures (500 and 600 °C) the second semicircle in mid-frequency range became clearer. The circuit used for fitting the impedance data can be written as  $R_s + R_1//Q_1 + R_2//Q_2$  (+ is for series and // for parallel connection), where  $R_s$  accounts for the electrolyte and contact resistance,  $R_1//Q_1$  are attributed to charge transport in the electrolyte and  $R_2//Q_2$  characterizes the  $Ni_{1-x}O$ /electrolyte interface. The fitting results are presented in the inset of Figure 5a. An example of fitting for sample 600 and the attributed circuit are presented in Fig. S1 from supplementary information. The charge transfer resistance ( $R_2$ ) decreases and capacity increases ( $Q_2$ ) with annealing temperature implying an increased conductivity/carrier concentration and thus narrower space charge layer thickness.

When the  $Ni_{1-x}O$  films are put into contact with the electrolyte, the equilibration of the Fermi level occurs along with majority carrier (holes) migration towards the interface. This produces a negative space charge layer in the semiconductor (also called depletion layer) and a positive space charge layer in the electrolyte (also called the Helmholtz layer), resulting in band bending. The separation of charge results in a measurable capacitance ( $C$ ) in the mid-frequency region, which comprises the contribution of the semiconductor space charge layer ( $C_{sc}$ ) and that of the Helmholtz layer ( $C_H$ ), i.e.  $C^{-1} = C_{sc}^{-1} + C_H^{-1}$ . The Nyquist plots (example given for sample 600 in Fig. 5b) and phase angle vs. frequency plots (example given for sample 600 in Fig. S2 from supplementary information) as function of applied bias represent additional evidence that it is the capacitive element in the mid-frequency region ( $Q_2$ ) that strongly changes as function of potential, and thus considered for the Mott-Schottky plot.

The electrolyte was prepared in order to be sufficiently concentrated (addition of 1M KCl) so that the Gouy layer [22] can be neglected. Since the  $C_H$  is considerably higher than the  $C_{sc}$  (the Helmholtz layer thickness is lower than the space charge layer thickness), the overall measured capacity is dominated by the space-charge capacitance ( $C_{sc}$ ) and its variation with the applied potential is described by the Mott-Schottky equation:

$$\frac{1}{C_{sc}^2} = -\frac{2}{e\epsilon\epsilon_0 N A^2} \left( E - \Phi_{fb} - \frac{kT}{e} \right) \quad (5)$$

where  $A$  is the effective surface area of the semiconductor (specific surface area evaluated from AFM [28] (140, 136, 32 and 22  $\text{m}^2/\text{g}$  for sample 350, 400, 500 and 600, respectively, see supporting information) and the entire film thickness were considered),  $E$  is the applied potential,  $\Phi_{\text{fb}}$  is the flat band potential,  $k$  is the Boltzman constant,  $T$  is the temperature in K,  $\epsilon$  is the dielectric constant of NiO (15, [29]),  $\epsilon_0$  is the vacuum permittivity,  $N$  is the carrier concentration within the depletion region and  $e$  is the electron charge. The Mott-Schottky plot corresponding to the 1.0 kHz frequency is shown in Fig. 6a. The space charge capacitance was found to be frequency dependent with a higher spreading for the sample annealed at 350 °C. The 1 kHz frequency was chosen from the scanned frequency range (15 kHz – 300 Hz) as saturation was achieved for all samples and because starting with this frequency the  $N/\Phi_{\text{fb}}$  dispersion was reduced [30] (as example the Mott-Schottky plots in the 1 kHz – 300 Hz range for samples 350 and 600 are shown in Fig.S3 from supplementary information). The intercept of the linear fit with the x axis (fit was done in the linear region) was used to determine the flat band potential whereas the carrier concentration was determined from the slope. Both carrier concentration and flat band potential values are summarized in Table 1. It can be clearly observed that the carrier concentration increases with annealing temperature along with flat band potential indicating a lowering of the valence band edge.

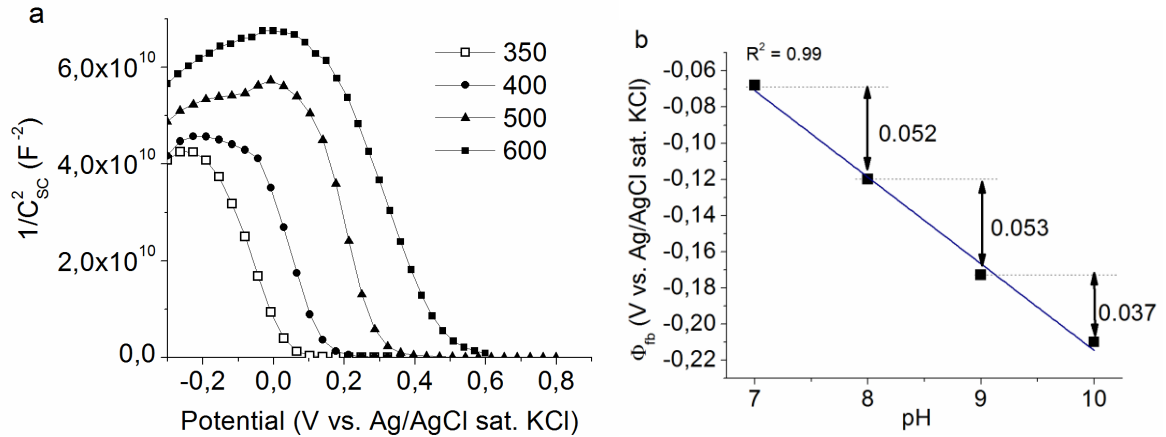


Fig. 6 Mott-Schottky plots for the 1.0 kHz frequency for the  $\text{Ni}_{1-x}\text{O}$  samples annealed at different temperatures (a) and the flat band variation as function of pH for the 350 case (b).

In addition, the Mott-Schottky plots were registered at different pH for the 350  $\text{Ni}_{1-x}\text{O}$  layer (Fig. 6b). The  $\Phi_{\text{fb}}$  value decreased with 0.052(3) V per unit of pH, which is close to the expected value of 0.059 V for an ideal semiconductor-aqueous electrolyte interface, meaning that suitable

measuring conditions were chosen. Exceptionally for the solution with pH 10 there was a higher deviation probably due to partial film dissolution.

Table 1. Effect of annealing temperature on the open circuit potential ( $V_{oc}$ ), carrier density ( $N$ ), flat-band potential ( $\Phi_{fb}$ ), valence band position ( $E_{VB}$ ), the potential at which the semiconductor is fully depleted ( $\Phi$  vs. Ag/AgCl and SHE), the potential drop across the space charge region ( $\Phi_{sc}$ ) and depletion layer thickness ( $L_{sc}$ ) of  $Ni_{1-x}O$  thin films.

Sample	$N$ ( $m^{-3}$ )	$V_{oc}$ (V/SHE)	$\Phi_{fb}$ (V/SHE)	$E_{VB}$ (eV/vacuum)	$\Phi$ (V vs. Ag/AgCl)	$\Phi$ (V /SHE)	$\Phi_{sc}$ (V/SHE)	$L_{sc}$ (nm)
350	$2.87 \cdot 10^{21}$	0.382	0.211	-4.64	-0.226	-0.027	0.185	292
400	$3.94 \cdot 10^{22}$	0.401	0.312	-4.74	-0.081	0.118	0.194	81
500	$5.80 \cdot 10^{23}$	0.432	0.467	-4.90	-0.008	0.191	0.276	25
600	$5.00 \cdot 10^{24}$	0.452	0.651	-5.08	0.031	0.230	0.421	10

When  $E < \Phi_{fb}$  the band bending increases, acting as a barrier for the passage of holes through the junction resulting in increased charge transfer resistance (the semicircle in the mid-frequency region increases at  $E < 0.4$  V, Fig. 5b), whereas for  $E > \Phi_{fb}$  the band bending is decreased favoring the holes diffusion and thus explaining the decrease in charge transfer resistance (the semicircle in the mid-frequency region almost disappears at  $E > 0.4$  V, Fig. 5b).

The open circuit potential ( $V_{oc}$ ) of each film (350, 400, 500 and 600) was measured with report to the Ag/AgCl sat. KCl reference electrode in the aqueous electrolyte (surface of electrode in contact with the electrolyte is  $0.15 \text{ cm}^2$ ) and values are given in Table 1. The  $V_{oc}$  increased with annealing temperature, indicating  $Ni^{3+}$  enrichment.

The valence band edge position can be calculated using the following equation for non-degenerated p-semiconductors [22]:

$$E_{VB} = \Phi_{fb} + \frac{kT}{e} \ln\left(\frac{N_V}{N}\right) \quad (6)$$

where  $N_V$  is the effective density of holes in the valence band defined as:

$$N_V = 2\left(\frac{2\pi m_h^* kT}{h^2}\right)^{3/2} \quad (7)$$

where  $h$  is the Planck constant and  $m_h^*$  is the effective mass of holes ( $0.9 m_0$  [31],  $m_0$  is the mass of an electron. Thus,  $N_V$  for  $Ni_{1-x}O$  is estimated to be  $2.1 \cdot 10^{19} \text{ cm}^{-3}$ . As already confirmed by the

flat band values the valence band edge can be tuned by annealing, i.e. lowered by increasing annealing temperature (Table 1) due to carrier concentration enhancement.

The width of the depletion layer ( $L_{sc}$ ) is given by:

$$L_{sc} = (2\epsilon\epsilon_0\Phi_{sc}/eN)^{1/2} \quad (8)$$

where  $e$  is the electron charge,  $\Phi_{sc}$  is the potential drop across the depletion region ( $\Phi_{sc} = \Phi_{fb} - \Phi$ , where  $\Phi$  is the potential at which  $Ni_{1-x}O$  layer is fully depleted and is determined from Fig. 6a at the turning point of the linear region towards negative region) and  $e$ ,  $N$ ,  $\epsilon$  and  $\epsilon_0$  have already been defined. The depletion layer width decreases with increasing carrier concentration and except for sample 350 for which it extends to the entire layer thickness (293 nm), for all the other samples it is confined at the layer surface, most probably due to reduced charged mobility.

The  $\Phi_{fb}$  and  $E_{VB}$  values are in good agreement with the values already reported for NiO films prepared by chemical solution processes [17,23,32]. The  $V_{oc}$  values are scarcely reported and they show the same trend as for our samples, i.e. increasing with  $Ni^{3+}$  concentration [14,15,20]. It is interesting to observe that lower  $V_{oc}$  values are reported for NiO films obtained by sputtering [14] which according to RBS analysis should have higher  $Ni^{3+}$  content when compared to our samples. Moreover, higher  $V_{oc}$  and transmission values are reported for NiO layers prepared by R.F. sputtering with 2% and 10%  $O_2$  [15] characterized by lower  $Ni^{3+}$  concentration as opposed to NiO layers prepared by D.C. sputtering with the same amount of oxygen and similar layer thickness [14].

### 3.4 Films conductivity

The films resistivity ( $\rho$ ) was measured by two points contact measurement in vertical geometry (contact surface  $0.8 \text{ mm}^2$ ) and used along with carrier concentration ( $N$ ) to calculate the mobility ( $\mu$ ) according to the formula:

$$\mu = \frac{1}{\rho Ne} \quad (9)$$

Film resistivity decreases (from 5.9  $k\Omega.cm$  for the sample 300 to 0.6  $k\Omega.cm$  for the sample 600) along with increasing carrier concentration and a radical drop in mobility was registered (0.36

$\text{cm}^2/(\text{V}\cdot\text{s})$  for sample 350 compared to  $0.0021\text{cm}^2/(\text{V}\cdot\text{s})$  for sample 600) which could be related to ionized impurity scattering (Fig. 7).

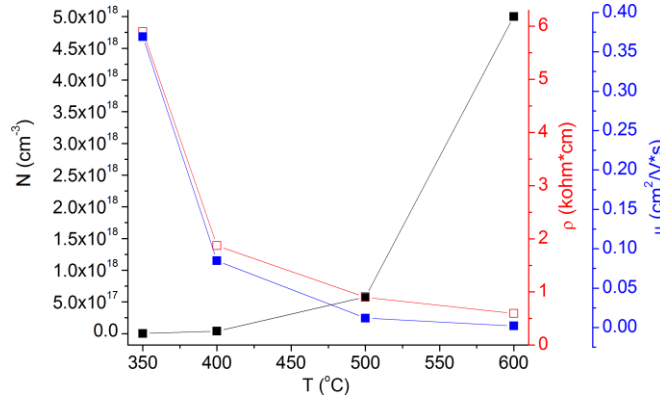


Fig. 7 Variation of the carrier concentration (N), resistivity ( $\rho$ ) and mobility ( $\mu$ ) of  $\text{Ni}_{1-x}\text{O}$  films as function of annealing temperature.

### 3.5 Stoichiometry and optical properties prediction

To begin, the  $V_{oc}$  values of the films (Table 1) were plotted versus the corresponding transmission values at 550 nm (Fig.8a) and a linear dependency was found. The correlation of optical and electrochemical parameters allows for determining the initial transmission of an unknown  $\text{Ni}_{1-x}\text{O}$  sample by simply dipping the film in the electrolyte and taking the  $V_{oc}$  value. When plotting the transmission or the open circuit potential vs. carrier concentration (Fig. 8b and c, respectively) linearity is again observed. It is to note that absorption values could also be used for building these curves. The inverse exercise could be made as well, for determining the transmission level of an unknown sample, carrier concentration or simply the  $V_{oc}$  have to be measured. The proposed method could be applied for determining the stoichiometry in  $\text{Ni}_{1-x}\text{O}$  films prepared by other methods, to Li-doped NiO, or other films which show important change in optical properties (either in the visible or near-infrared region) with carrier concentration/stoichiometry modification (i.e. highly sub-stoichiometric titanium oxide or transparent conducting oxides).



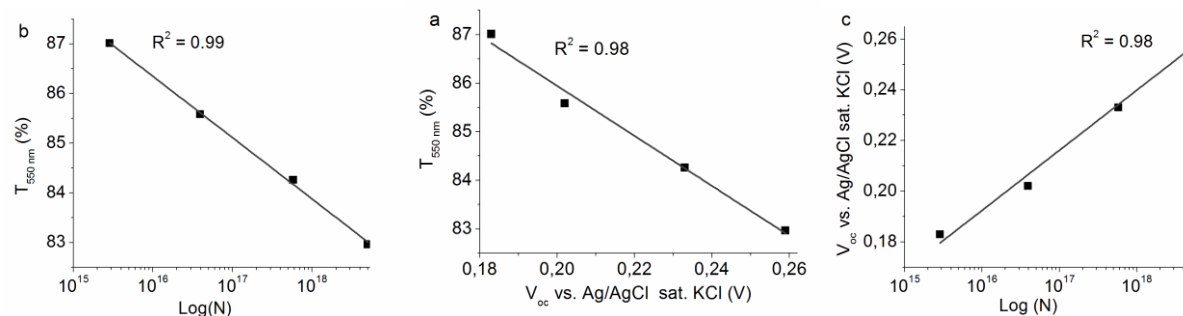


Fig. 8 Transmission (at 550 nm) vs. the open circuit potential  $V_{oc}$  (a), transmission (at 550 nm) vs. carrier concentration (b), and open circuit potential  $V_{oc}$  vs. carrier concentration (c).

Such correlations have never been done before and allow for the straightforward determination of the carrier concentration and stoichiometry by measuring film transmission or  $V_{oc}$  since  $x$  in  $\text{Ni}_{1-x}\text{O}$  is given by [33]:

$$x = \frac{[V_{\text{Ni}}] \cdot M}{\rho \cdot N_A} \quad (10)$$

where nickel vacancy concentration  $[V_{\text{Ni}}]$  is equal to carrier concentration  $N$  if we consider that all the vacancies are ionized ( $N_A$  is the Avogadro number, and  $\rho$  and  $M$  are the NiO density and molar mass). The  $x$  values for sample 300, 400, 500 and 600 are given in Table 2 next to the number of  $\text{Ni}^{3+}$  sites per unit cell ( $\text{Ni}^{3+}$  MS) obtained by considering that for one nickel vacancy two  $\text{Ni}^{3+}$  sites are formed (eq.1).

Table 2. Stoichiometry variation with annealing temperature.

Sample	$x_{\text{MS}}$	$\text{Ni}^{3+}_{\text{MS}}$	$\text{Ni}^{3+}_{\text{CV}}$	$\text{Ni}^{3+}/(\text{Ni}^{2+} + \text{Ni}^{3+})$	$x_{\text{XPS}}$	$\text{Ni}^{3+}_{\text{XPS}}$
350	$0.5 \cdot 10^{-7}$	$0.1 \cdot 10^{-6}$	$3.5 \cdot 10^{-5}$	-	-	-
400	$0.7 \cdot 10^{-6}$	$1.5 \cdot 10^{-6}$	$3.6 \cdot 10^{-5}$	0.054	0.010	0.020
500	$1.0 \cdot 10^{-5}$	$2.0 \cdot 10^{-5}$	$1.2 \cdot 10^{-5}$	-	-	-
600	$3.7 \cdot 10^{-5}$	$7.4 \cdot 10^{-5}$	$1.4 \cdot 10^{-4}$	0.137	0.016	0.032

MS – Mott-Schottky analysis, CV – cyclic voltammetry and XPS – X-ray spectroscopy analysis

To verify our theory, we registered the transmission spectra of a  $\text{Ni}_{1-x}\text{O}$  sample which was annealed at 500 °C for 8 h in Ar atmosphere and used the calibration curve in fig. 8b to determine the carrier concentration. For a transmission level of 85.8% at 550 nm,  $N$  was found to be  $2.2 \cdot 10^{16} \text{ cm}^{-3}$ . The  $V_{oc}$  was also measured (0.195 V vs. Ag/AgCl sat. KCl) as previously described and lead to similar carrier concentration when extrapolated in Fig. 8c. At the same

time the carrier concentration was determined by Mott-Schottky measurements (Fig. S4 in supplementary information), in the same conditions as all the other samples, giving a similar value i.e.  $N = 2.3 \cdot 10^{16} \text{ cm}^{-3}$ . Furthermore, the carrier concentration of the sample annealed at 500 °C in Ar atmosphere ( $2.2 \cdot 10^{16} \text{ cm}^{-3}$ ) was lower than the one of the same sample annealed in air ( $5.8 \cdot 10^{17} \text{ cm}^{-3}$ ), as expected.

For comparison, the number of  $\text{Ni}^{3+}$  sites was also determined by performing a cathodic scan of fresh non-cycled films in 0.5 M  $\text{LiClO}_4$  in PC electrolyte at 20 mV/s scan rate (Fig. 9), starting from the equilibrium potential towards -0.5 V vs. Ag/AgCl (3M KCl saturated with AgCl) reference electrode and ending when cathodic current reached 0.

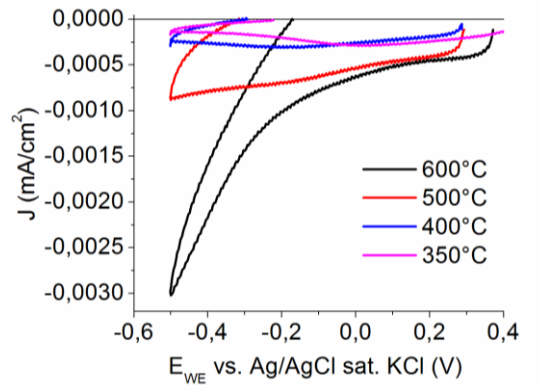


Fig. 9 First reduction curves of the  $\text{Ni}_{1-x}\text{O}$  samples in 0.5 M  $\text{LiClO}_4$  in PC electrolyte (specific surface was considered).

The charge capacity was extracted from the electrochemical curves for all the samples by integration and further used for calculating the number of  $\text{Ni}^{3+}$  sites (eq.12) [14].

$$\text{Ni}^{3+}\text{CV} = \frac{Q}{A} * \frac{M}{ed\rho N_A} \quad (11)$$

The number of  $\text{Ni}^{3+}$  sites determined by cathodic scan is higher than the one derived from the Mott-Schottky plots. These differences might originate from the used scanning speed as the surface of cyclic voltammetry and thus the charge capacity modifies with scanning speed, or from a trace contamination of the electrolyte or sample.

Likewise, for comparison purposes, a physical method i.e. XPS was used for determining the degree of non-stoichiometry in the samples 400 and 600. The core level spectra of the Ni  $2p_{3/2}$

states for the 400 and 600 Ni<sub>1-x</sub>O thin films are presented in Fig. 10a and b, respectively. The binding energy at 853.9 eV is attributed to the Ni 2p<sub>3/2</sub> main peak, the shoulder at 856.1/856.2 eV is the surface component, and the binding energies at 855.3/855.4 eV are indexed to Ni<sup>3+</sup> states. Meanwhile, the binding energies at 861.0 and 863.7/863.8 eV were attributed to the charge transfer satellite peaks [26,34].

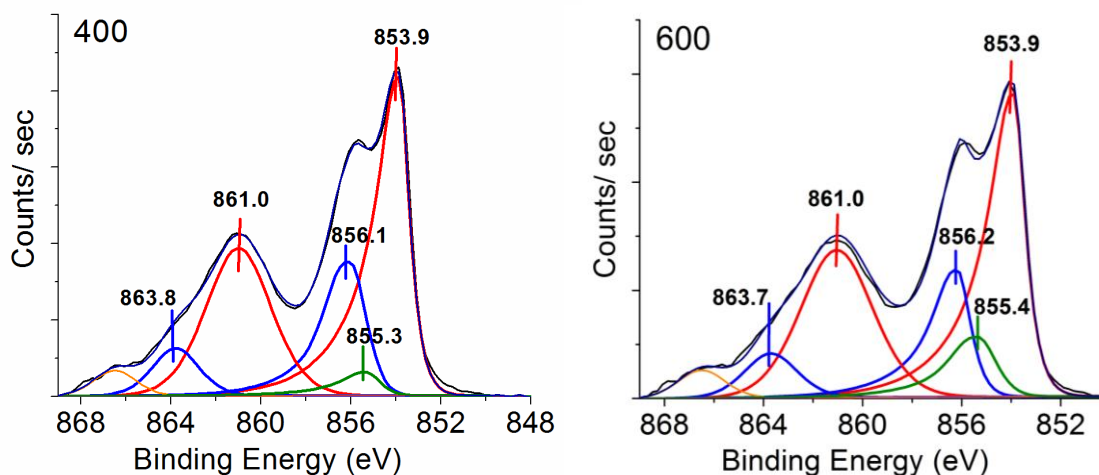


Fig. 10 Fig. 10 XPS spectra of the Ni 2p<sub>3/2</sub> states in Ni<sub>1-x</sub>O thin films annealed at 400 (a) and 600 °C (b) along with the deconvolution.

The Ni<sup>3+</sup>/(Ni<sup>3+</sup> + Ni<sup>2+</sup>) ratios, the Ni<sup>3+</sup> concentration and consequently the “x” values were calculated with respect to the Ni<sup>2+</sup> (853.9 eV) and Ni<sup>3+</sup> (855.3 and 855.4 eV) peaks for the sample 400 and 600, respectively) and values were included in Table 2. Based on the XPS quantification the formula of the Ni<sub>1-x</sub>O films can be written as Ni<sub>0.90</sub>O or Ni<sub>0.97</sub><sup>2+</sup>Ni<sub>0.02</sub><sup>3+</sup>O in the case of sample 400, and Ni<sub>0.84</sub>O or Ni<sub>0.984</sub><sup>2+</sup>Ni<sub>0.032</sub><sup>3+</sup>O for sample 600. It can be clearly observed that by XPS considerably higher Ni<sup>3+</sup> concentrations are obtained compared to Mott-Schottky analysis for both samples.

### 3.6 Comparison with literature

In view of the difference in “x” values between the electrochemical and XPS analysis, a literature survey was undertaken concerning the different methods for determining the stoichiometry of Ni<sub>1-x</sub>O films synthesized by chemical or physical processes (Table 3). In addition, wherever carrier concentration was given we have calculated the x values (assuming a constant value for the layer density and molar mass) by using the eq. 11, and compared the results with our own (the values are written in **bold** in Table 3).

Table 3. Literature survey on x determination in  $\text{Ni}_{1-x}\text{O}$  films prepared by different methods. Layer thickness (d), transmission at 550 nm ( $T_{550 \text{ nm}}$ ), carrier concentration (N), flat band potential ( $\Phi_{fb}$ ), open circuit potential ( $V_{oc}$ ) and valence band edge position ( $E_{VB}$ ) are also given.

Ref.	Deposition method/ heat treatment	d [nm]	$T_{550 \text{ nm}}$ [%]	x value/ method	N [cm <sup>-3</sup> ]	$\Phi_{fb}$ vs. SHE [V]/ media/ pH	$E_{VB}$ [eV]	$V_{oc}$ vs. SHE [V]
20	PLD, $PO_2=10^{-1}$ mbar	30	80-95	-	-	-	-	0.68
25	Spin coating, 400 °C in air	906	32	<b><math>2.4 \cdot 10^{-4}</math></b>	$1.3 \cdot 10^{19}/2\text{-P}$	-	-	-
	Spin coating, 700 °C in air	500	11	<b><math>6.9 \cdot 10^{-4}</math></b>	$3.7 \cdot 10^{19}/2\text{-P}$	-	-	-
16	Spray pyrolysis, 400 °C in air	350	75	0.56/ XPS <b><math>3.3 \cdot 10^{-5}</math></b>	$1.8 \cdot 10^{17}/$ 4-p HE	-	-	-
22	ALD, 300 °C in Ar atm.	71	85	<b><math>0.2 \cdot 10^{-5}</math></b>	$1.1 \cdot 10^{17}/ \text{MS}$	0.19/ aq/ 10	-5.2	-
	ALD, 300 °C in O <sub>2</sub> atm.	71	-	<b><math>5.0 \cdot 10^{-4}</math></b>	$2.7 \cdot 10^{19}/ \text{MS}$	0.69/ aq/ 10	-5.2	-
	ALD, 600 °C in O <sub>2</sub> atm.	71	-	<b>0.14</b>	$7.3 \cdot 10^{21}/ \text{MS}$	0.73/ aq/ 10	-5.2	-
17	Spray pyrolysis, 450 °C in air	100	70	<b><math>9.1 \cdot 10^{-4}</math></b>	$4.9 \cdot 10^{19}/ \text{MS}$	0.36/naq/10	-4.8	-
32	Blade coating, 450 °C in air	600	-	0.55/ XPS <b><math>2.2 \cdot 10^{-5}</math></b>	$1.2 \cdot 10^{18}/ \text{MS}$	0.37/ aq/ 7	-4.8	-
18	R.F. sputtering, 30% O <sub>2</sub>	100	-	0.006/ RBS vs. 0.020/ XPS	-	-	-	-
	R.F. sputtering, 100% O <sub>2</sub>	100	-	0.05/ RBS vs. 0.027/XPS	-	-	-	-
12	R.F. sputtering, 6% O <sub>2</sub>	360	-	0.076/ XPS I vs. 0.13/ XPS II	-	-	-	-
	R.F. sputtering, 80% O <sub>2</sub>	360	-	0.083/ XPS I vs. 0.19/ XPS II	-	-	-	-
14	D.C. sputtering, 2% O <sub>2</sub>	300	84	0.16/ RBS	-	-	-	0.13
	D.C. sputtering, 10% O <sub>2</sub>	300	62	0.32/ RBS	-	-	-	0.23
15	R.F. sputtering, $PO_2=2\%$	250	92	0.009/ CV	-	-	-	0.54
	R.F. sputtering, $PO_2=10\%$	250	44	0.035/ CV	-	-	-	0.84
26	R.F. sputtering, Ar atm.	900	55	0.19/ XPS	-	-	-	-
23	Electrodep., 400 °C in air	-	-	<b><math>3.3 \cdot 10^{-2}</math></b>	$1.8 \cdot 10^{21}/ \text{MS}$	0.50/ aq/ 10	-4.9	-
35	R. F. sputtering, $PO_2=10\%$	60	50	<b><math>1.0 \cdot 10^{-2}</math></b>	$5.5 \cdot 10^{21}/$ 4-p HE	-	-	-
36	R. F. sputtering, $PO_2=10^{-4}$ mbar	-	60	<b><math>0.5 \cdot 10^{-5}</math></b>	$2.6 \cdot 10^{17}/$ 4-p HE	-	-	-
19	R.F. sputtering, $PO_2=50\%$ ,	100	-	0.44/ XPS <b><math>3.3 \cdot 10^{-2}</math></b>	$1.8 \cdot 10^{21}/4\text{-p}$ HE	-	-	-
	R.F. sputtering, $PO_2=50\%$ , 100 °C in N <sub>2</sub>	100	-	0.36/ XPS <b><math>4.6 \cdot 10^{-3}</math></b>	$2.5 \cdot 10^{20}/4\text{-p}$ HE	-	-	-
This study	Spray pyrolysis, 400 °C in air	200	86	<b><math>0.7 \cdot 10^{-6}</math></b> 0.2•10 <sup>-4</sup> / CV 0.010/ XPS	$3.9 \cdot 10^{16}/ \text{MS}$	0.31/ aq/ 7	-4.7	0.40
	Spray pyrolysis, 600 °C in air	200	83	<b><math>3.7 \cdot 10^{-5}</math></b> 0.7•10 <sup>-4</sup> / CV 0.016/ XPS	$5.0 \cdot 10^{18}/ \text{MS}$	0.65/ aq/ 7	-5.0	0.45

MS – Mott-Schottky measurement, HE – Hall Effect measurement, 2-P – two point measurements, 4-P four point measurement in Van der Paw configuration, CV – cyclic voltammetry.

When looking at the table we first note that different techniques applied on the same sample render very different results [18]. Even more, there are significant differences reported for the same technique. Chen et. al [12] extracted higher x values from the O/Ni ratio than from the  $\text{Ni}^{3+}/\text{Ni}^{2+}$  ratio and explained this by  $\text{Ni}^{3+}$  enrichment at the surface of nanostructures.

It is likely possible that the difference comes from not removing the O related to organic contamination. Usually the content of  $\text{Ni}^{3+}$  determined by XPS is higher compared to values obtained by RBS, cycling voltammetry or the values calculated by our approach. A very thin layer of  $\text{Ni}(\text{OH})_2$  [20] could be present at the film surface which is not detected by RBS leading to x overestimation.

Some contradictions are also found, the x value determined from cyclic voltammetry curves [15] is smaller (0.035) than the x value obtained by RBS [14] (0.32, considering that for each oxygen interstitial one nickel vacancy is formed) for NiO film with similar thickness, even if the transmission level at 550 nm is lower (44% vs. 62%, respectively), suggesting higher  $\text{Ni}^{3+}$  content.

Regarding our method for assessing x, we see that by applying it to other groups samples similar results are obtained when dealing with same range of carrier concentrations [16,22,32], validating our results. Moreover, for higher carrier concentrations ( $10^{20}$ - $10^{21}$   $\text{cm}^{-3}$ ) the values calculated by our method come near the x values determined by XPS or RBS [19,22,23,35] validating our approach.

### 3.7 Electrochromic activity

Since initially the films were intended for EC applications, the evaluation of their performance is investigated in a non-aqueous electrolyte. The electrochromic behavior of the two samples representing the extremes in terms of annealing temperatures (samples 350 and 600) were tested in the 0.5M  $\text{LiClO}_4$  in PC electrolyte in the -0.5 – 1.2V potential range by cyclic voltammetry (CV) at 20 mV/s scan rate. The *in situ* cycling of the as-deposited  $\text{Ni}_{1-x}\text{O}$  samples, previously performed in our group [2], showed that the bleaching was finished at around -0.5 V vs Ag/AgCl sat KCl. For more negative potentials (going up to -1.4 V) no change in optical and electrochemical capacity were registered. The 10<sup>th</sup> CV cycle is shown fig. 11a.

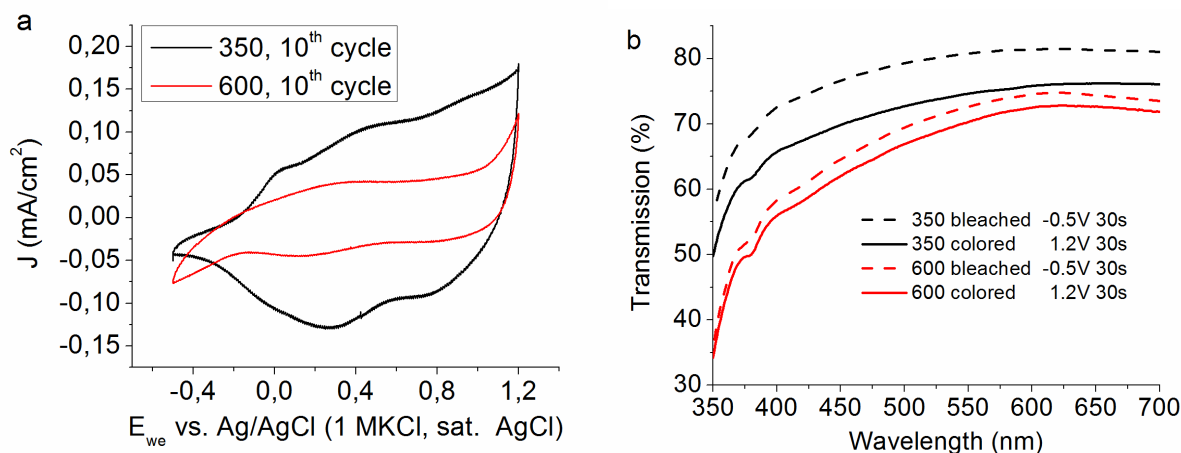


Fig. 11 Cyclic voltammetry curves (a) and colored and bleached state transmission spectra (b) of the samples 350 and 600.

The surface of the CV for the sample 350 is largely higher compared to that of sample 600. The transmission spectra of the 350 and 600 samples in the colored and bleached state are shown in fig. 11b. It can readily be observed that sample 600 (richer in  $Ni^{3+}$  sites) has a lower transmission modulation and that the transmission in the colored and bleached state are lower compared to sample 350. This is in agreement with other reports [2,14,15] which show that the colored and bleached state transmission of  $Ni_{1-x}O$  films are progressively lower with increasing  $x$ .

The stoichiometry results show that the sample 600 has a higher  $Ni^{3+}$  concentration than sample 300 and should thus have a higher transmission modulation. However, the electrochromic experiments show the contrary. The lower performance was attributed to the layer structure. In fact sample 600 is more crystalline according to XRD results and has lower specific surface. This is in agreement with previous studies [12,37] which link the reduced transmission modulation to the increasing layer crystallinity and compactness which hampers  $Li^+$  ions diffusion.

#### 4. Conclusions

Compact p-type  $Ni_{1-x}O$  layers with  $0.7 \cdot 10^{-6} < x < 3.7 \cdot 10^{-5}$  (and corresponding  $N$  values of  $3.9 \cdot 10^{16}$  and  $5.0 \cdot 10^{18}$ ) were synthesized by ultrasonic spray pyrolysis (USP) and subsequently annealed in air at 350, 400, 500 and 600 °C. The  $Ni^{3+}$  content in the films increased with rising annealing temperature as confirmed by XRD, optical absorption and Mott-Schottky analysis.

Giving the low  $x$  values, we conclude that NiO films with higher carrier concentration can only be prepared by USP when doping is used or by physical methods. The  $x$  values determined by electrochemical measurements were significantly lower compared to XPS values. This leads us to conclude that the elemental analysis of non-stoichiometric oxides is challenging from the point of view of selecting the appropriate analysis tool and the accurate and universal interpretation of results.

The particle size increases with increasing annealing temperature resulting in increased film compactness, as proven by the rising contact angle values, and consequently to decreasing specific surface. The changes in specific surface were taken into consideration during the electrochemical analysis. A lower electrochromic performance was obtained for films with higher  $\text{Ni}^{3+}$  concentration due to the increased film compactness and crystallinity. Film conductivity is increased (hole concentration enhances) with rising temperature leading to a lower charge transfer resistance at the electrolyte/ $\text{Ni}_{1-x}\text{O}$  interface.

The original correlation *transmission (T)-open circuit potential ( $V_{oc}$ )-carrier concentration (N)* demonstrated in this study allowed the straightforward evaluation of stoichiometry in unknown  $\text{Ni}_{1-x}\text{O}$  films and the prediction of their optical properties. The transmission in the initial, colored and bleached state is lowered with increasing  $x$ . The  $V_{oc}$  is a valuable material property as information about stoichiometry can be obtained by simply following its evolution, i.e.  $V_{oc}$  increases for decreasing  $x$  values.

## Acknowledgements

The authors are thankful to the Walloon Region of Belgium for the funding of the Exactacoat Ultrasonic Spray Pyrolysis equipment through the SMARTSPRAY project (n°1117339, Greenomat). Laura Manceri is grateful to the Walloon Region and AGC Flatglass ("Nouveaux produits CVD" Project, Convention de sous-traitance n°7428) for post-doctoral financial support. Anthony Maho thanks "Fonds de la Recherche Scientifique" (FNRS) for post-doctoral financial support (FC 86864). The authors would also like to thank Gilles Sronck (GREENMat) for films deposition and Cédric Malherbe (Analytical Chemistry and Electrochemistry Departement, University of Liège,) for optical measurements.

## 5. References

- [1] M. Mihelčič, A. Šurca Vuk, I. Jerman, B. Orel, F. Švegl, H. Moulki, C. Faure, G. Campet, A. Rougier, Comparison of electrochromic properties of  $\text{Ni}_{1-x}\text{O}$  in lithium and lithium-free aprotic electrolytes: From  $\text{Ni}_{1-x}\text{O}$  pigment coatings to flexible electrochromic devices, *Sol. Energ. Mat. & Sol. Cells* 120 (2014) 116-130.
- [2] J. Denayer, G. Bister, P. Simonis, P. Colson, A. Maho, P. Aubry, B. Vertruyen, C. Henrist, V. Lardot, F. Cambier, R. Cloots, Surfactant-assisted ultrasonic spray pyrolysis of nickel oxide and lithium-doped nickel oxide thin films, toward electrochromic applications, *Appl. Surf. Sci.* 321 (2014) 61-69.
- [3] I. Hod, Z. Tachan, M. Shalom, A. Zaban, Characterization and control of the electronic properties of a NiO based dye sensitized photocathode *Phys. Chem. Chem. Phys.* 15 (2013) 6339-6343.
- [4] Y.-C. Lin, Y.-T. Chen, P.-C. Yao, Effect of post-heat-treated NiOx overlayer on performance of nanocrystalline  $\text{TiO}_2$  thin films for dye-sensitized solar cells, *J. Power Sources* 240 (2013) 705-712.
- [5] S. Ozdemir, T.B. Osburn, J.L. Gole, Nanostructure modified gas sensor detection matrix for NO transient conversion of NO to  $\text{NO}_2$ , *J. Electrochem. Soc.* 158 (2011) J201-J207.
- [6] J. Zhang, D. Zeng, Q. Zhu, J. Wu, Q. Huang, C. Xie, Effect of nickel vacancies on the room-temperature  $\text{NO}_2$  sensing properties of mesoporous NiO nanosheets, *J. Phys. Chem. C* 120 (2016) 3936–3945.
- [7] H. Long, G. Fang, H. Huang, X. Mo, W. Xia, B. Dong, X. Meng, X. Zhao, Ultraviolet electroluminescence from ZnO/NiO-based heterojunction light-emitting diodes, *Appl. Phys. Lett.* 95 (2009) 013509(1-3).
- [8] M. Tyagi, M. Tomar, V. Gupta, Postdeposition annealing of NiOx thin films: A transition from n-type to p-type conductivity for short wave length optoelectronic devices, *J. Mater. Res.* 28 (2013) 723-732.



- [9] A. Stokłosa, Defect complexes and defect clusters in  $\text{Mn}_{1-\delta}\text{O}$ ,  $\text{Co}_{1-\delta}\text{O}$  and  $\text{Ni}_{1-\delta}\text{O}$  oxides diagrams of the concentrations of point defects, *Int. J. Chem.* 4 (2012) 1-25.
- [10] H.G. Sockel, H. Schmalzried, Coulometric titration of transition metal oxides, *Ber. Bunsenges. Phys. Chem.* 72(7) (1968) 745-754.
- [11] P. Lunkenheimer, A. Loidl, C.R. Otterman, K. Bange, Correlated barrier hopping in NiO films, *Phys. Rev. B* 44 (1991) 5927-5930.
- [12] T.F. Chen, A.J. Wang, B.Y. Shang, Z.L. Wu, Y.L. Li, Y.S. Wang, Property modulation of NiO films grown by radio frequency magnetron sputtering, *J. Alloys Comp.* 643 (2015) 167-173.
- [13] S. Nandy, B. Saha, M. K. Mitra, Effect of oxygen partial pressure on the electrical and optical properties of highly (200) oriented p-type  $\text{Ni}_{1-x}\text{O}$  films by DC sputtering, *J. Mater. Sci.* 42, (2007) 5766-5772.
- [14] R.-T. Wen, C.G. Granqvist, G.A. Niklasson, Anodic electrochromism for energy-efficient windows: cation/anion-based surface processes and effects of crystal facets in nickel oxide thin films, *Adv. Funct. Mat.* 25 (2015) 3359-3370.
- [15] M. Da Rocha, A. Rougier, Electrochromism of non-stoichiometric NiO thin film: as single layer and in full device, *Applied Physics A* 122:370 (2016) 1-7.
- [16] C.-C. Wu, C.-F. Yang, Effect of annealing temperature on the characteristics of the modified spray deposited Li-doped NiO films and their applications in transparent heterojunction diode, *Sol. Energ. Mat. & Sol. Cells* 132 (2015) 492–498.
- [17] X.H. Chan, J.R. Jennings, M.A. Hossain, K.K.Z. Yu, Q. Wang, Characteristics of p-NiO thin films prepared by spray pyrolysis and their application in CdS-sensitized photocathodes, *J. Electrochem. Soc.* 158 (2011) H733 – H740.
- [18] D.S. Kim, H.C. Lee, Nickel vacancy behavior in the electrical conductance of nonstoichiometric nickel oxide film, *J. Appl. Phys.* 112 (2012) 034504(1-4).

- [19] J.-L. Yang, Y.-S. Lai, J.S. Chen, Effect of heat treatment on the properties of non-stoichiometric p-type nickel oxide films deposited by reactive sputtering, *Thin Solid Films* 488 (2005) 242 – 246.
- [20] I. Bouessay, A. Rougier, P. Poizot, J. Moscovici, A. Michalowicz, J.-M. Tarascon, Electrochromic degradation in nickel oxide thin film: A self-discharge and dissolution phenomenon, *Electrochim. Acta* 50 (2005) 3737–3745.
- [21] M. Rubin, S.-J. Wen, T. Richardson, J. Kerr, K. von Rottkay, J. Slack, Electrochromic lithium nickel oxide by pulsed laser deposition and sputtering, *Sol. Energ. Mat. & Sol. Cells* 54 (1998) 59-66.
- [22] E. Thimsen, A.B.F. Martinson, J.W. Elam, M.J. Pellin, Energy Levels, Electronic properties and rectification in ultrathin p-NiO films synthesized by atomic layer deposition, *J. Phys. Chem. C* 12 (2012) 16830-16840.
- [23] K. Nakaoka, J. Ueyama, K. Ogura, Semiconductor and electrochromic properties of electrochemically deposited nickel oxide films, *Journal of electroanalytical chemistry* 571 (2004) 93–99.
- [24] W.-J. An, E. Thimsen, P. Biswas, Aerosol-chemical vapor deposition method for synthesis of nanostructured metal oxide thin films with controlled morphology, *J. Phys. Chem. Lett.* 1 (2010) 249-253.
- [25] S.R. Nalage, M.A. Chougule, S. Sen, P.B. Joshi, V.B. Patil, Sol-gel synthesis of nickel oxide thin films and their characterization, *Thin Solid Films* 520 (2012) 4835–4840.
- [26] K.S. Usha, R. Sivakumar, C. Sanjeeviraja, V. Sathe, V. Ganesan and T. Y. Wang, Improved electrochromic performance of a radio frequency magnetron sputtered NiO thin film with high optical switching speed, *RSC Adv.* 6 (2016) 79668-79680.
- [27] Y. Qing, C. Yang, Z. Yu, Z. Zhang, Q. Hu, C. Liu, Large-Area Fabrication of Superhydrophobic Zinc Surface with Reversible Wettability Switching and Anticorrosion, *J. Electrochem. Soc.* 163 (8) (2016) D385-D391.

- [28] J. Antony, J. Nutting, D.R. Baer, D. Meyer, A. Sharma, Y. Qiang, Size-dependent specific surface area of nanoporous film assembled by core-shell iron nanoclusters, *J. Nanomat.* 2006 (2006) 1-4.
- [29] R. Newman, R. M. Chrenko, Optical properties of nickel oxide, *Physical Reviews* 114 (1959) 1507-1513.
- [30] R. Ramesham, Determination of flat-band potential for boron-doped diamond electrode in 0.5 m NaCl by ac-impedance spectroscopy, *Thin Solid Films* 322 (1998) 158-166.
- [31] S.C. Choi, K. Koumoto, H. Yanagida, Electrical conduction and effective mass of a hole in single-crystal NiO, *J. Mater. Sci.* 21 (1986) 1947-1950.
- [32] G. Natu, P. Hasin, Z. Huang, Z. Ji, M. He, Y. Wu, Valence band-edge engineering of nickel oxide nanoparticles via cobalt doping for application in p-type dye-sensitized solar cells, *ACS Appl. Mater. Interfaces* 4 (2012) 5922 – 5929.
- [33] O.T. Sørensen, Nonstoichiometric oxides. Chap. 1 Thermodynamics and defect structure of nonstoichiometric oxides, Academic Press INC. (1981), pg 2-56.
- [34] I. Preda, A. Gutierrez, M. Abbate, F. Yubero, J. Mendez, L. Alvarez, L. Soriano, Interface effects in the Ni 2p x-ray photoelectron spectra of NiO thin films grown on oxide substrates, *Phys. Rev. B* 77 (2008) 075411 1-7.
- [35] Y. Chen, Y. Sun, X. Dai, B. Zhang, Z. Ye, M. Wang, H. Wu, Tunable electrical properties of NiO thin films and p-type thin-film transistors, *Thin Solid Films* 592 (2015) 195–199.
- [36] A.M. Reddy, A.S. Reddy, K. Lee, P.S. Reddy, Effect of oxygen partial pressure on the structural, electrical and optical properties of sputtered NiO films, *Ceram. Int.* 37 (2011) 2837–2843.
- [37] Z. Chen, A. Xiao, Y. Chen, C. Zuo, S. Zhou, L. Li, Highly porous nickel oxide thin films prepared by a hydrothermal synthesis method for electrochromic application, *J. Phys. Chem. Solids* 74 (2013) 1522-1526.